Hindawi
International Journal of Antennas and Propagation
Volume 2022, Article ID 5307430, 14 pages
https://doi.org/10.1155/2022/5307430

Research Article

Design and Analysis of UWB MIMO Antenna for Smart Fabric Communications

Thennarasi Govindan,[1] **Sandeep Kumar Palaniswamy**,[1] **Malathi Kanagasabai**,[2] **and Sachin Kumar**[1]

[1]*Department of Electronics and Communication Engineering, SRM Institute of Science and Technology, Kattankulathur 603203, India*
[2]*Department of Electronics and Communication Engineering, College of Engineering, Anna University, Guindy, Chennai 600025, India*

Correspondence should be addressed to Sandeep Kumar Palaniswamy; vrpchs@gmail.com

Received 6 November 2022; Revised 30 November 2022; Accepted 13 December 2022; Published 21 December 2022

Academic Editor: Ravi Gangwar

This paper presents a flexible multiple-input, multiple-output (MIMO) antenna with ultrawideband (UWB) performance for smart clothing applications. The MIMO antenna is comprised of four octagonal-shaped radiators with several slots loaded into them, and it offers a frequency range of 2.9–12 GHz. The unit cell has a size of $0.26\lambda_0 \times 0.164\lambda_0 \times 0.014\lambda_0$ and the MIMO antenna has a size of $0.48\lambda_0 \times 0.48\lambda_0 \times 0.014\lambda_0$, where λ_0 corresponds to the lowest operating frequency. The radiation and diversity performances of the antenna are evaluated, and the obtained metrics are envelope correlation coefficient (ECC) <0.045, diversity gain (DG) >9.9 dB, total active reflection coefficient (TARC) <−14 dB, and channel capacity loss (CCL) <0.13 bits/s/Hz. The bending analysis of the MIMO antenna is performed. The specific absorption rate (SAR) of the MIMO antenna is also investigated, and the obtained values are 0.229 W/Kg (4 GHz), 0.253 W/Kg (7 GHz), and 0.463 W/Kg (10 GHz).

1. Introduction

In recent years, smart clothing has gained popularity for wearable electronic gadgets such as watches, buttons, military berets, sunglasses, and so on [1]. Wearable electronics attached to textiles should be flexible and conformal for on-body applications. This inspires the development of smart clothing, where wearable antennas are used to transmit/receive data [2]. Wearable antennas are widely used in the medical, military, and healthcare industries, as well as in fashion design and aesthetics [3]. In [4], a 2.4 GHz planar inverted-F antenna (PIFA) was presented for security applications. However, it has the disadvantage of a narrow bandwidth. The development of a compact, wide-coverage antenna is essential for wearable applications. In [5], a semicircular slot antenna was designed on a lower dielectric substrate material for ultrawideband (UWB). The substrate material used in antenna design is important for wearable applications, and a low-loss substrate material can improve antenna efficiency. Another important factor is the relative permittivity of the substrate, and a substrate with a lower dielectric constant reduces surface wave losses and improves wave propagation [6]. In [7], a textile-based wearable antenna was designed with a polyester substrate, and the impact of the weaving process was evaluated. A conformal spiral antenna made of conductive elektrisola e-threads that operates at 1–3 GHz frequency was presented in [8]. In [9], a dual-port embroidery textile antenna was designed for military applications. The literature [10–13] reported antenna designs using a variety of flexible substrates such as polydimethylsiloxane (PDMS), denim, jeans, cotton, jute, and felt. These antennas are inexpensive and simple to integrate into fashionable clothing.

It is difficult to create a wideband textile antenna that can reliably transmit data even when the human body's posture changes. Multiple-input, multiple-output (MIMO) antennas

could be used to address such issues [14]. MIMO antennas have several advantages over a single antenna in terms of increased data rate, improved system reliability, and quality [15]. The only drawback of MIMO systems is the mutual coupling between antenna elements. Mutual coupling degrades the antenna's performance by interfering with nearby signals. Mutual coupling can be reduced by using periodic structures, such as an electromagnetic bandgap (EBG), an artificial magnetic conductor (AMC), and a frequency selective surface (FSS) [16–18]. In [17], a metamaterial-based AMC structure was developed on a polyester substrate to improve bandwidth and interelement isolation. These aspects, however, increase the complexity of the antenna structure [19]. There are some simple strategies for improving isolation, such as adding slits and slots or decoupling structures [20], introducing parasitic elements between the radiators [21], and a defected ground structure [22]. Furthermore, mutual coupling can be effectively reduced by adding meander lines to the ground plane [23]. The orthogonal architecture of antennas leads to minimization of mutual coupling, as reported in [24]. Also, keeping a sufficient spacing between the antenna elements can also help to reduce mutual coupling without the use of any decoupling mechanisms.

In this study, the design and development of a UWB MIMO flexible antenna for smart fabric applications are presented. Smart fabric refers to integration of antennas to the body outfits that track the movements and collect biometric data, such as body temperature, heart rate, and pulse rate which could be helpful for patient monitoring, location tracking, and security applications [25]. The proposed work uses cotton fabric for a textile antenna, and the proposed MIMO antenna's effectiveness is assessed using surface current distribution and diversity metrics. The proposed quad-port MIMO antenna provides an impedance bandwidth of 9.1 GHz (2.9–12 GHz) and a maximum gain of 4.84 dBi. The bending study is used to evaluate the flexibility of the proposed antenna, which can be bent up to a bending angle of 143.3°. SAR analysis is performed to assess its impact on the human body, and the obtained SAR values are well below 1.6 watts/kg. The flexibility of the developed antenna makes it potentially useful in applications such as patient monitoring and healthcare.

2. Antenna Design

2.1. Unit Cell Design. Figure 1 shows the design of the proposed octagonal-shaped UWB monopole antenna. The antenna is designed on the cotton textile (dielectric constant = 1.6; loss tangent = 0.04) substrate material with a thickness of $0.014\lambda_0$ [6]. Cotton is preferred for antenna design because of its strength and durability. Also, it stretches easily and is weather-resistant and water-repellent. It is highly recommended for people with skin allergies due to its hypoallergenic properties. Cotton material is widely used in hospitals for curtains, pillows, and patient clothing [26]. The designed antenna is made of cotton material and works as a textile antenna when integrated with a patient cloth. The size of the unit cell is $0.26\lambda_0 \times 0.164\lambda_0 \times 0.014\lambda_0$. The designed antenna operates in the frequency range of 3.1–12 GHz.

The proposed antenna design began with an octagonal-shaped patch and a partial ground plane of length $0.038\lambda_0$, as shown in Figure 2(a). Figure 3 depicts the reflection coefficient plots at four stages of evolution. It covers an impedance bandwidth of 0.7 GHz (3.1–3.8 GHz) and 4.75 GHz (7.25–12 GHz). In evolution stage 2, the ground plane is lengthened to $0.07\lambda_0$ and truncated on both sides by $0.0048\lambda_0$ (Figure 2(b)). As a result, the reflection coefficient curve covers the frequency of 3.1–3.8 GHz in the lower frequency region and extends from 6.7 to 12 GHz in the higher frequency region. In the next stage, three sides of the octagonal radiator are truncated (Figure 2(c)) to lower the impedance in the lower frequency range. In the fourth evolution stage, a rectangular stub of length $0.029\lambda_0$ and width $0.048\lambda_0$ is introduced (Figure 2(d)) between the octagonal radiator and feedline. It increases the electrical length of the radiating element and results in a broad bandwidth of 8.9 GHz (3.1–12 GHz).

The current distribution is investigated in order to better understand the radiation performance of the antenna. Figure 4 depicts the surface current distribution at 4 GHz and 10 GHz. The current is distributed in the feedline to achieve the lowest operating frequency as shown in Figure 4(a). The current is highly dispersed in the circular slot, two octagonal slots, feedline, and around the radiator's circumference at 10 GHz, as shown by the reflection coefficient curves.

The monopole antenna's lowest operating frequency (f_l) is determined by using the following equation [27]:

$$f_l = \frac{7.2}{(l_m + b_m + p_m) \times k}, \tag{1}$$

where l_m and b_m are the length and width of the monopole radiator and the distance between the monopole radiator and the ground plane is denoted by p_m which is equivalent to 0.25 cm. k is related to the effective dielectric constant to the power of 0.5.

Rewrite equation (1) as (2) to equate it to the perimeter of the octagonal radiator.

$$f_l = \frac{7.2}{\left(1.217\pi\left[(s_l + s_w)\right] + p_g\right) \times k}. \tag{2}$$

The term $(l_m + b_m)$ is rewritten as $1.46\pi(s_l + s_w)$, which is the perimeter of an octagonal radiator. s_l and s_w are the semilength and semiwidth of the octagonal radiator.

For better understanding the physical characteristics of the proposed antenna, equivalent circuit is illustrated in Figure 5. The analogous circuit is made up of the R, L, and C components. The series and parallel arrangements of the R, L, and C components are determined from the real and imaginary curves shown in Figure 6. Serial connection is made if the real and imaginary curves move from low to high, and parallel connection is made if these curves travel from high to low [28]. The simulated S11 curve shows the deep resonance at 3.6, 7.8, and 10.8 GHz frequencies throughout the entire UWB. Therefore, the serial and

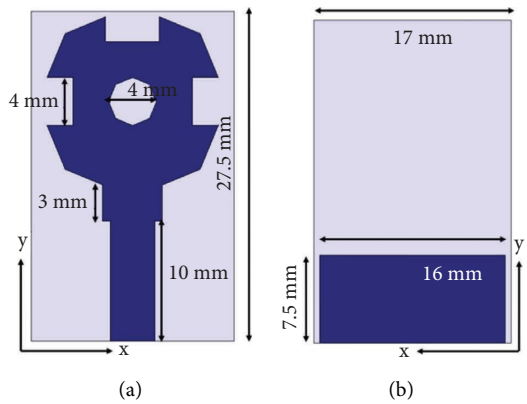

Figure 1: Layout of the monopole antenna: (a) front side and (b) back side.

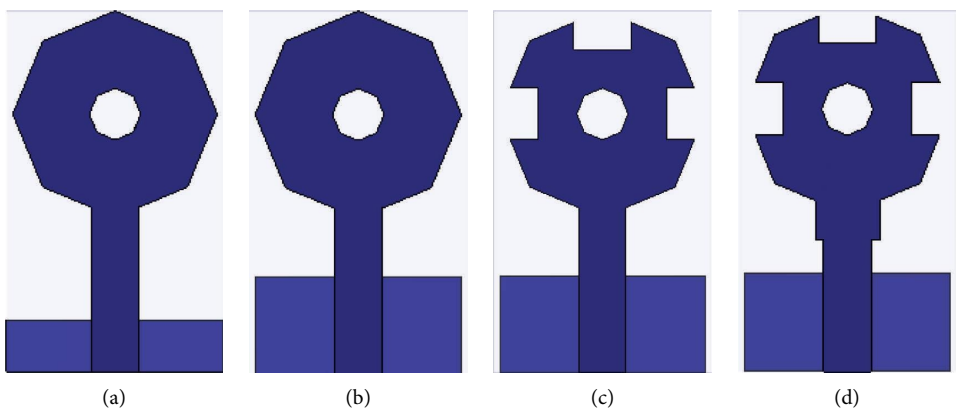

Figure 2: Development stages of the antenna: (a) evolution 1, (b) evolution 2, (c) evolution 3, and (d) evolution 4.

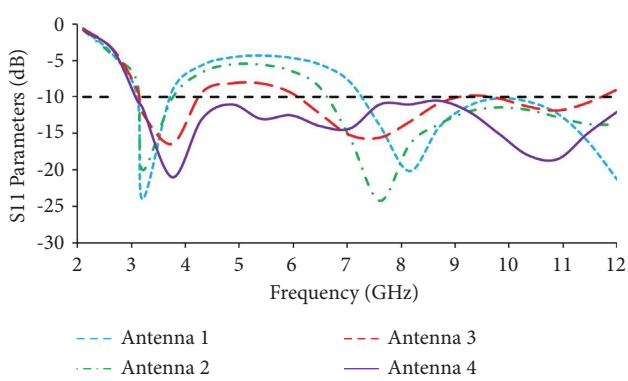

Figure 3: Reflection coefficients at various stages of evolution.

parallel arrangements of R, L, and C components are constructed at these three frequencies. At 3.6 and 10.8 GHz frequencies, the real and imaginary impedance curves move from high to low, resulting in a parallel configuration of R, L, and C components. However, at 7.8 GHz, the real and impedance curves shift from low to high, resulting in a serial configuration of R, L, and C components.

The S11 curve obtained from the equivalent circuit is compared with the simulated S11 curve as depicted in Figure 7. The simulated reflection coefficient curve shows an impedance bandwidth of 8.9 GHz (3.1–12 GHz), whereas the reflection coefficient obtained from the equivalent circuit shows an impedance bandwidth of 8.8 GHz (3.1–11.9 GHz).

2.2. MIMO Antenna Design. Figure 8 depicts the layout of the MIMO antenna. The octagonal-shaped antenna elements are transformed into a quad-port MIMO antenna, with each element positioned orthogonally to the other. The spacing between the antennas is retained as $0.07\lambda_0$ for good isolation. The MIMO antenna occupies a total area of $0.48\lambda_0 \times 0.48\lambda_0 \times 0.014\lambda_0$. The designed antenna is fabricated, as shown in Figure 9, and its S-parameters are measured using an Agilent MS 2037C vector network analyzer.

3. Results and Discussion

3.1. Transmission and Reflection Characteristics. Figures 10 and 11 depict the simulated and measured S-parameter curves of the antenna. The simulated and measured impedance bandwidths of the MIMO antenna are 8.9 GHz (3.1–12 GHz) and 9.1 GHz (2.9–12 GHz), respectively. The reflection coefficient plots for Antenna-1 and Antenna-3 are identical. In the same way, Antenna-2 and Antenna-4 have similar

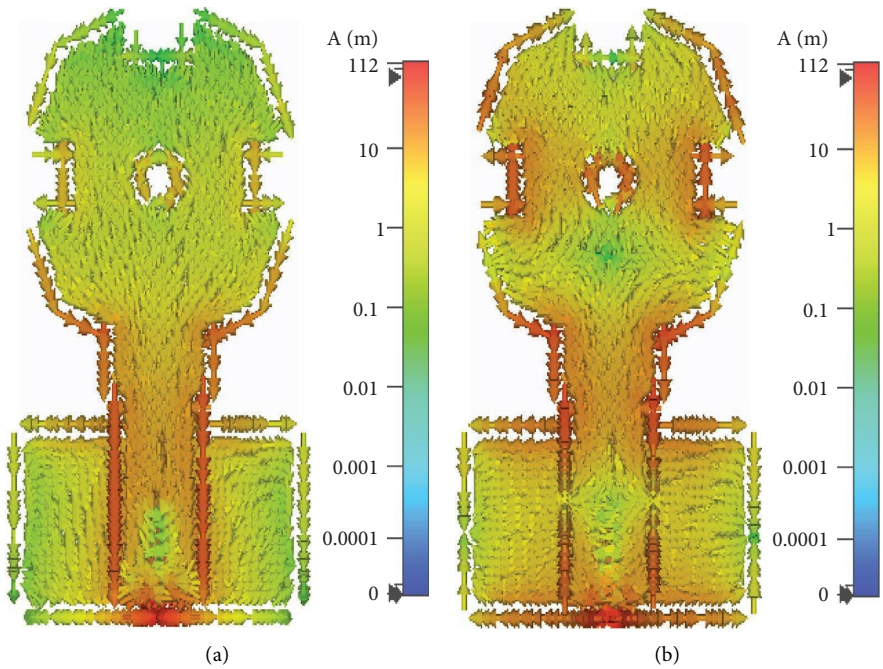

Figure 4: Current distribution at (a) 4 GHz and (b) 10 GHz.

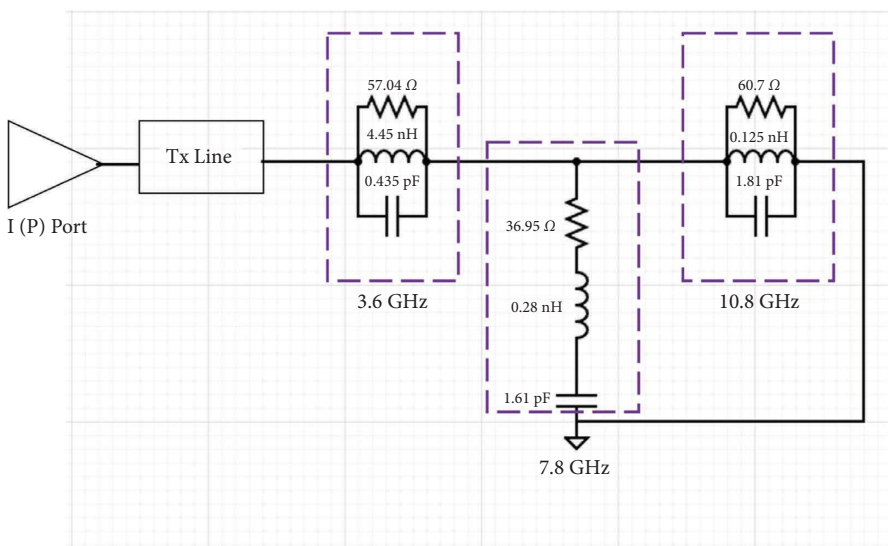

Figure 5: Equivalent circuit plot of the proposed antenna.

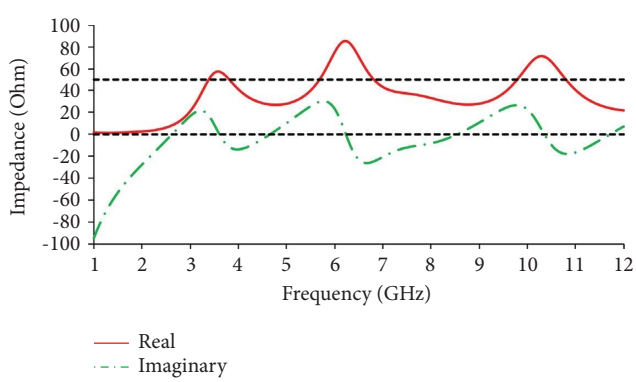

Figure 6: Real and imaginary impedance characteristics of the proposed antenna.

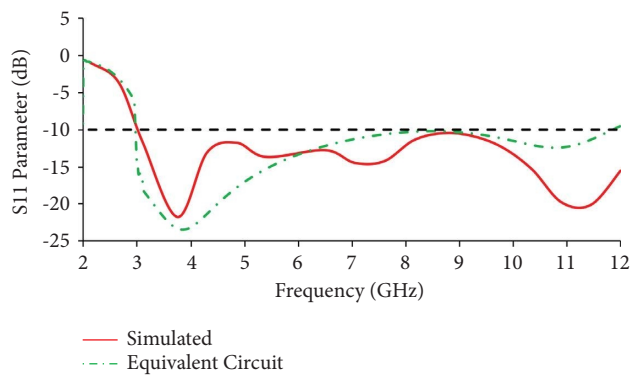

Figure 7: Reflection coefficient comparison of simulated and equivalent circuits.

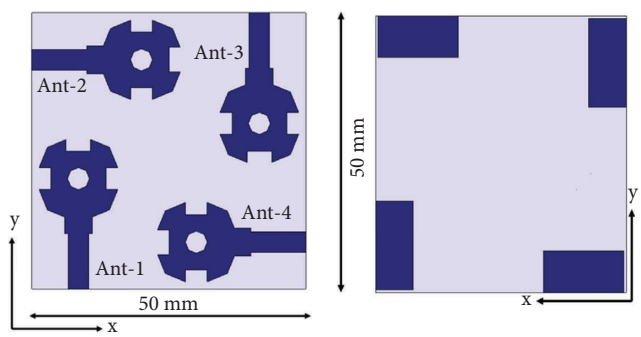

(a) (b)

Figure 8: Layout of the MIMO antenna: (a) radiator and (b) ground plane.

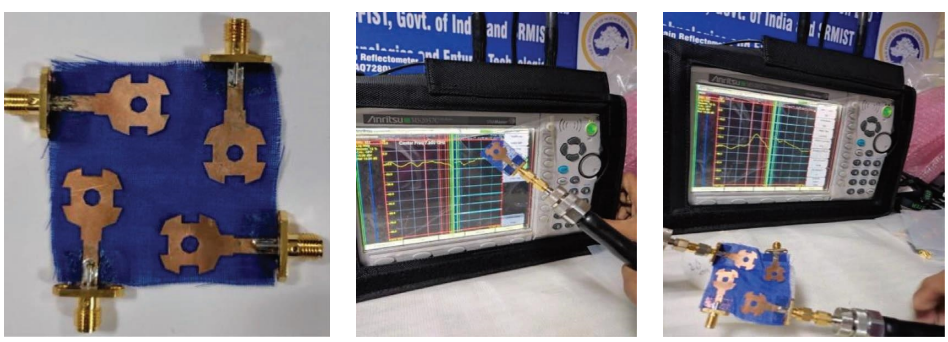

(a) (b) (c)

Figure 9: (a) Prototype of the MIMO antenna, (b) unit cell measurement using VNA, and (c) MIMO antenna measurement using VNA.

reflection coefficient curves. Without the use of decoupling structures, an isolation of >17 dB is achieved across the UWB range.

3.2. Radiation Performance. The antenna is kept inside the anechoic chamber, and its radiation characteristics, such as gain and patterns, are measured. When port-1 is enabled, the adjacent ports (ports-2, -3, and -4) are matched with a 50-ohm impedance. When port-2 is excited, all other ports are matched, and vice-versa. The radiation patterns of the proposed antenna are plotted at three different frequencies in the E-plane ($\phi = 90^\circ$) and H-plane ($\phi = 0^\circ$). The radiation pattern curves appear bidirectional in the E-plane and omnidirectional in the H-plane. The radiation pattern is plotted for both free-space and on-body conditions. As illustrated in Figure 12, the radiation performance of the antenna is reduced in the presence of a human body when compared to the free-space condition due to the lossy behavior of the human tissues.

Figure 13 depicts the efficiency and gain curves of the proposed antenna. The observed simulated gain values are 2.83 dBi for 3 GHz, 3.54 dBi for 6 GHz, and 4.84 dBi for 10 GHz whereas the measured gains at 3 GHz, 6 GHz, and 10 GHz are 2.5 dBi, 3.2 dBi, and 4.5 dBi, respectively. The maximum efficiency achieved is 91.6%.

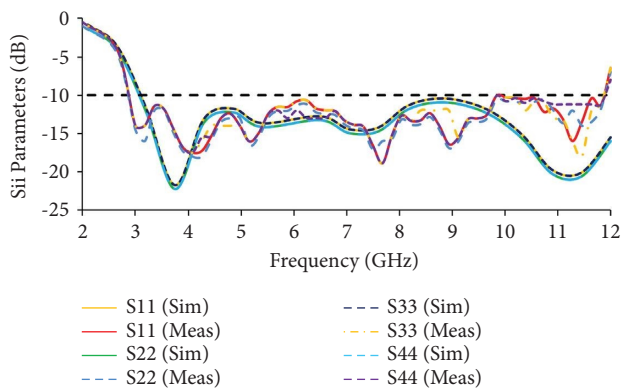

Figure 10: S_{ii}-plots of the proposed MIMO antenna.

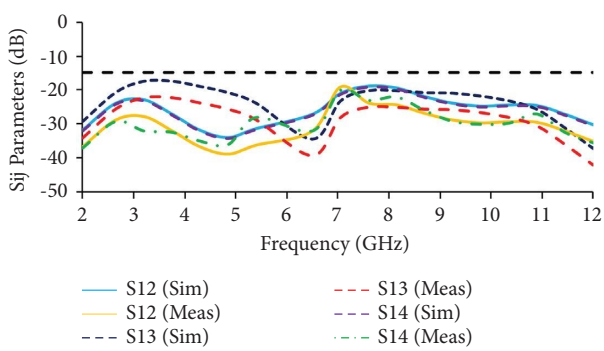

Figure 11: S_{ij}-plots of the proposed MIMO antenna.

3.3. Bending Analysis. Textile antennas should be flexible and capable of working in bending situations [29]. To meet this requirement, the proposed MIMO antenna is tested in a variety of bending scenarios. Figure 14 depicts the simulated bending analysis of the proposed antenna with different bending radius ($r = 25$ mm, $r = 20$ mm, and $r = 15$ mm). Figure 15 depicts the measured bending analysis of the MIMO antenna. The developed antenna performs well in both simulated and measured scenarios, covering the entire UWB spectrum, as shown in Figure 16. The performance of the proposed MIMO antenna begins to degrade at bending radius $r = 15$ mm.

The critical bending angle is the bend angle at which the antenna performance starts to degrade.

Bending angle (θ) of the antenna is calculated using the following equation [30]:

$$\text{bending angle}\,(\theta) = \frac{h_y \times 360}{br \times 2\pi}, \tag{3}$$

where br is the bending radius and h_y is the length of the antenna in the y-plane. The bending angles obtained at three different bending radiuses (25 mm, 20 mm, 15 mm) are 114.64°, 143.3°, and 191.08°.

These bending angles reveal that the proposed MIMO antenna can be bent up to 143.312° without altering its working performance. However, at the bending angle of 191.08°, the performance of the proposed MIMO antenna starts to deteriorate, which is the critical angle. Therefore, the critical angle of the proposed MIMO antenna is 191.08°.

3.4. Diversity Performance. The evaluation of diversity metrics is important for MIMO antenna. One of them is the envelope correlation coefficient (ECC), which provides correlation information between adjacent unit cells [31]. It can be calculated using the following equation [32]:

$$\text{ECC} = \frac{\left|\int\int\left[\overrightarrow{F_1}(\theta,\varphi).\overrightarrow{F_2}(\theta,\varphi)\right]d\Omega\right|^2}{\int\int\left|\overrightarrow{F_1}(\theta,\varphi)\right|^2 d\Omega \int\int\left|\overrightarrow{F_2}(\theta,\varphi)\right|^2 d\Omega}, \tag{4}$$

where F_1 and F_2 are the radiated fields obtained from the radiation patterns and (θ, φ) are elevation and azimuth angles varying between $0 \le \theta \le \pi$ and $0 \le \varphi \le 2\pi$.

Another diversity parameter is diversity gain (DG). It defines how well a signal is transmitted with the minimum loss during transmission [33]. It can be calculated using the following equation [34]:

$$\text{DG} = \sqrt{1 - |\text{ECC}|^2}. \tag{5}$$

Figure 17 depicts the DG and ECC graphs of the MIMO antenna using the far field. The total active reflection coefficient (TARC) is also used to calculate the diversity performance of the antenna. It is the square root of the sum of the total reflected waves (b_i) divided by the square root of the total incident waves (a_i).

$$\text{TARC} = \frac{\sqrt{\sum_{i=1}^{N}|b_i|^2}}{\sqrt{\sum_{i=1}^{N}|a_i|^2}}. \tag{6}$$

TARC can be calculated for a two-port antenna using the following equation:

$$\text{TARC} = \Gamma_a^t = \frac{\sqrt{\left(\left|S_{11} + S_{12}e^{j\theta}\right|^2\right) + \left(\left|S_{21} + S_{22}e^{j\theta}\right|^2\right)}}{\sqrt{2}}. \tag{7}$$

Channel capacity loss (CCL) defines transmission loss in high-data-rate transmission [35]. CCL is calculated using the following equation:

$$\text{CCL} = -\log_2 |\psi|^R, \tag{8}$$

where $|\psi|^R = \begin{vmatrix} \rho_{11} & \rho_{12} \\ \rho_{21} & \rho_{22} \end{vmatrix}$ is the correlation matrix and

$$\begin{aligned} \rho_{11} &= \left(1 - |S_{11}|^2 - |S_{12}|^2\right), \\ \rho_{12} &= -\left(S_{11}{}^* S_{12} + S_{21}{}^* S_{12}\right), \\ \rho_{21} &= -\left(S_{22}{}^* S_{21} + S_{12}{}^* S_{21}\right), \\ \rho_{22} &= \left(1 - |S_{22}|^2 - |S_{21}|^2\right). \end{aligned} \tag{9}$$

Figure 18 depicts the TARC and CCL plots of the MIMO antenna.

3.5. SAR Analysis. Specific absorption rate (SAR) is the ratio of absorbed power to unit mass.

$$\text{SAR} = \frac{\text{d}}{\text{d}t}\left(\frac{dW}{\rho dV}\right)\left(\frac{\text{W}}{\text{kg}}\right), \tag{10}$$

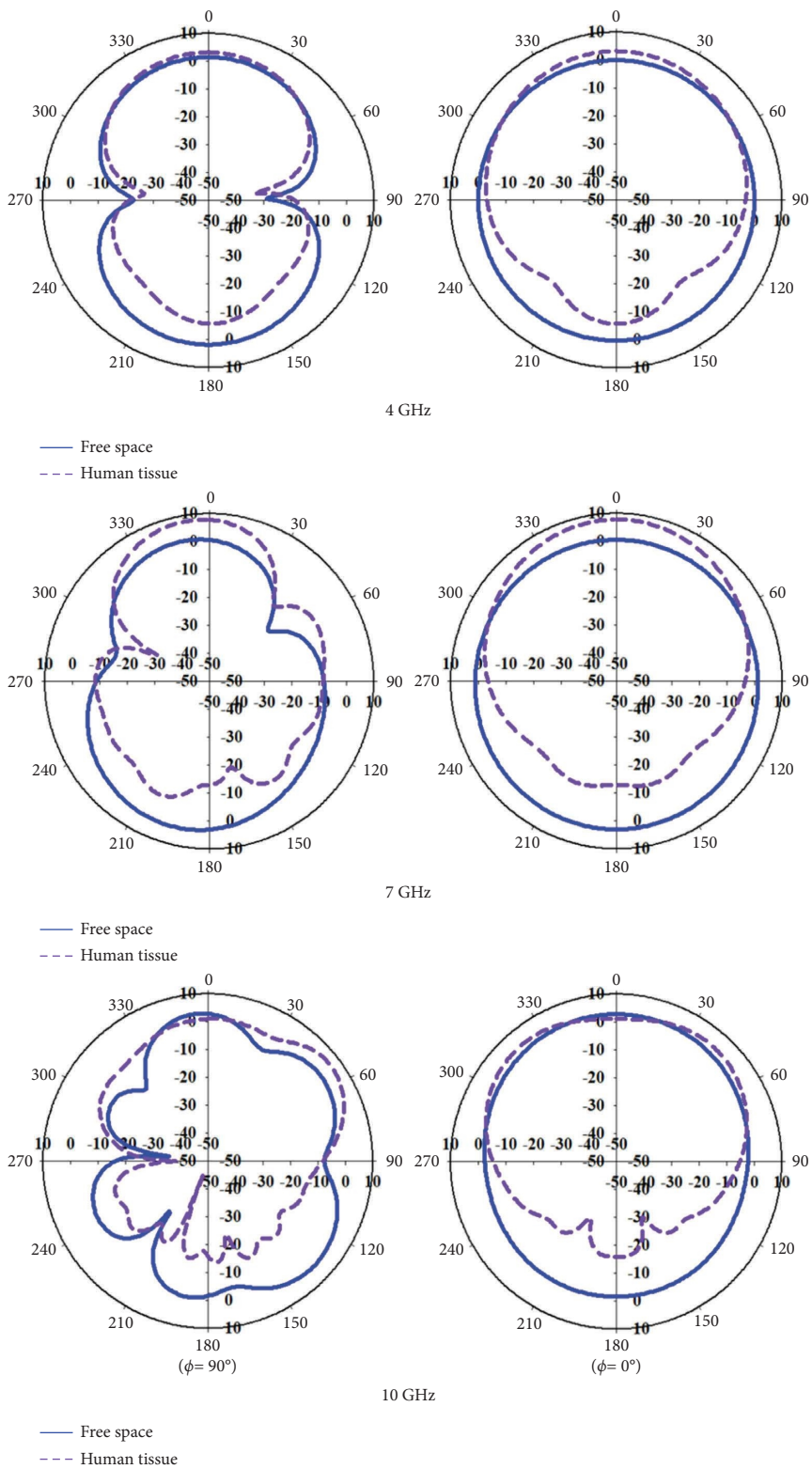

Figure 12: Radiation patterns of the proposed MIMO antenna.

where W denotes the amount of energy absorbed by human tissue, V denotes the sample volume, and ρ is the mass density [36]. The proposed antenna is kept on 100 mm × 100 mm rectangular human body tissue model, as shown in Figure 19(a).

Table 1 lists the tissue properties of the human body [37]. The input power is set at 1 watt. As shown in Figure 19(b), the SAR values obtained are 0.229 W/Kg at 4 GHz, 0.253 W/Kg at 7 GHz, and 0.463 W/Kg at 10 GHz. The designed antenna is also tested by inserting it into three different body

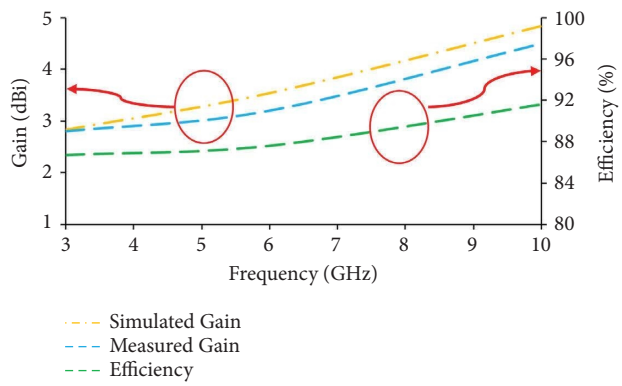

Figure 13: Gain and efficiency plots of the antenna.

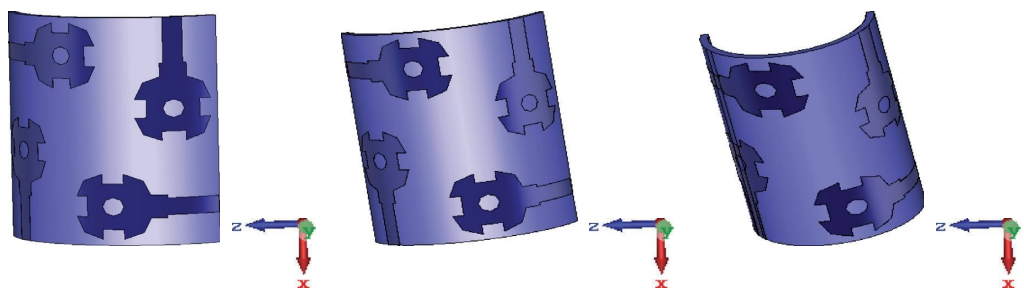

(a) (b) (c)

Figure 14: Simulated bending analysis of the MIMO antenna: (a) $r = 25$ mm, (b) $r = 20$ mm, and (c) $r = 15$ mm.

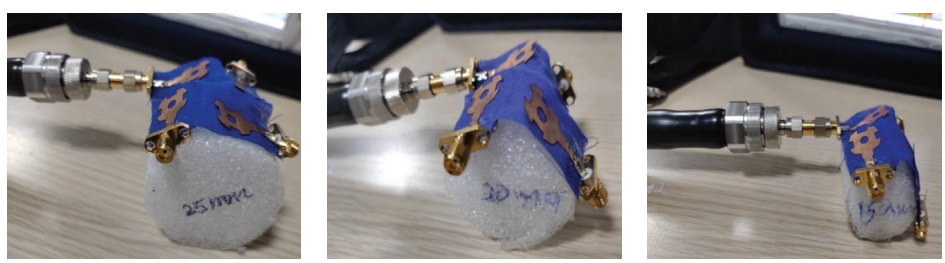

(a) (b) (c)

Figure 15: Bending analysis of the fabricated MIMO antenna: (a) $r = 25$ mm, (b) $r = 20$ mm, and (c) $r = 15$ mm.

parts of the open-source imported model [38], and the SAR values are shown in Figure 20. Figure 21 depicts the reflection coefficient curves for the on-body scenario of the MIMO antenna. It covers an impedance bandwidth of 8.5 GHz (3.1–11.6 GHz).

The antenna is tested for on-body performance by placing it on the human body. Figure 22 depicts the measured S-parameter results, which show an impedance bandwidth of 9.9 GHz (2.1–12 GHz). Figure 23 depicts the reflection coefficient curves plotted in free space and on the human body. The reflection coefficient curves do not change when the antenna is placed on the human body.

Table 2 compares the performance of the developed antenna to the existing literature.

(i) When compared to previous studies, the proposed octagonal unit cell has a smaller area of $0.26\lambda_0 \times 0.164\lambda_0$

(ii) In contrast to [7, 29] and [39–43], which are designed for narrowband frequencies, the proposed antenna is designed for wideband frequencies

(iii) The proposed antenna has a wide bandwidth of 8.9 GHz, whereas the impedance bandwidths offered by [7, 29] and [39–43] are narrow

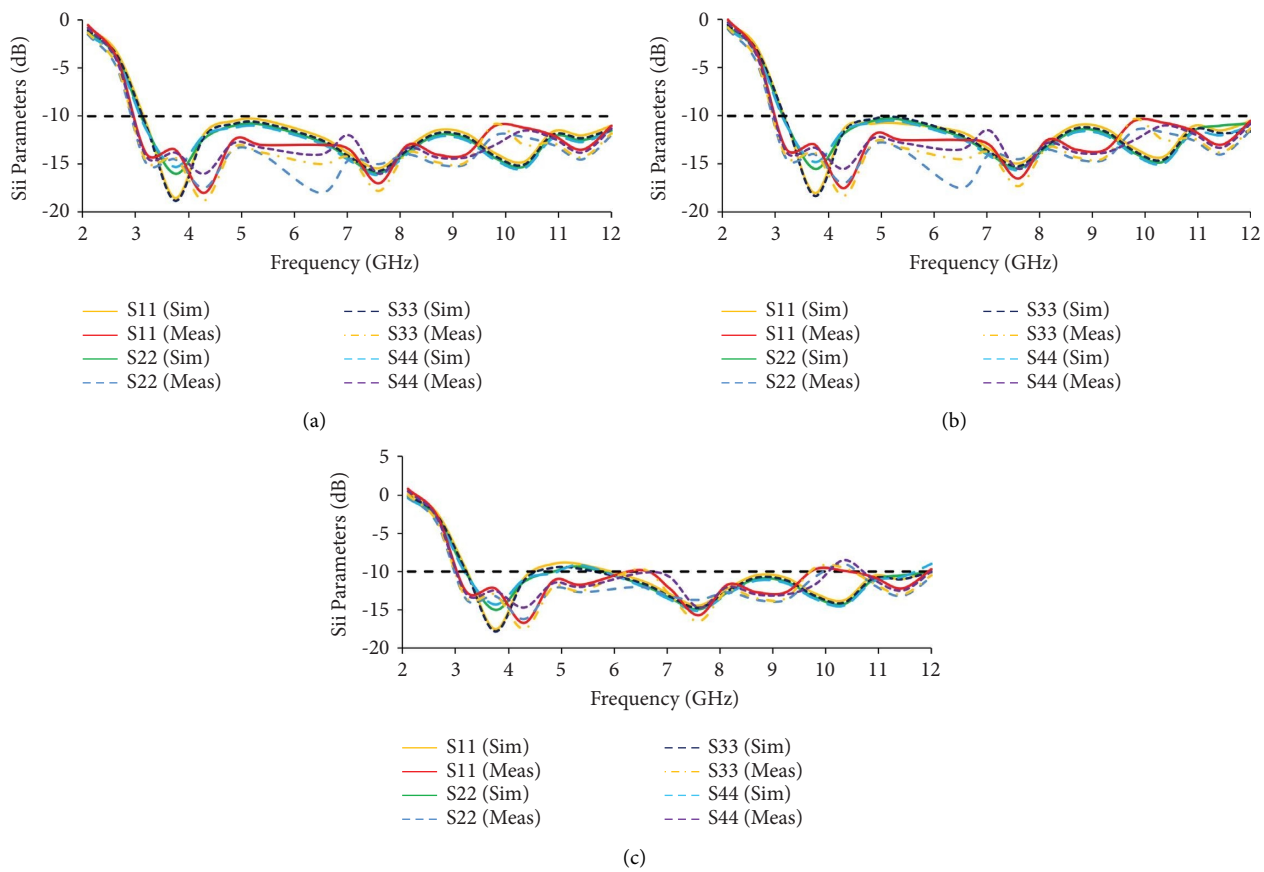

Figure 16: Reflection coefficient plots in different bending scenarios: (a) $r = 25$ mm, (b) $r = 20$ mm, and (c) $r = 15$ mm.

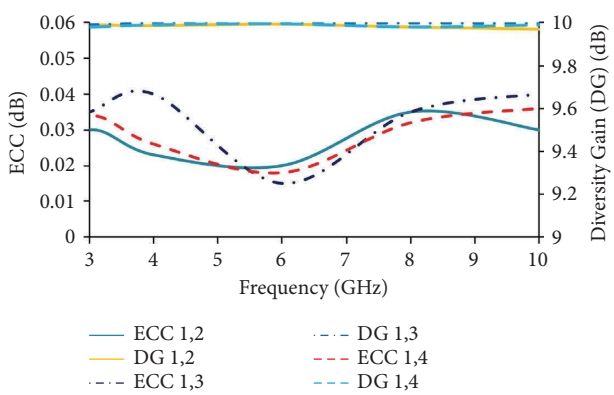

Figure 17: ECC and DG plots of the MIMO antenna.

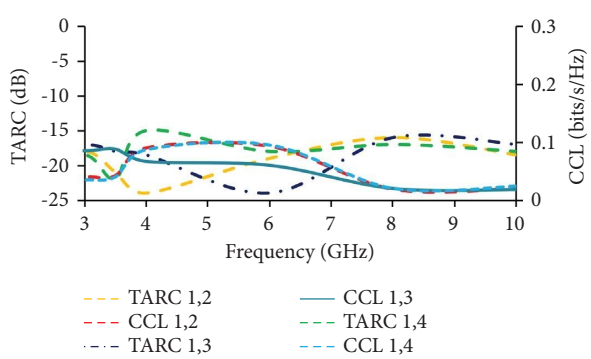

Figure 18: TARC and CCL plots of the MIMO antenna.

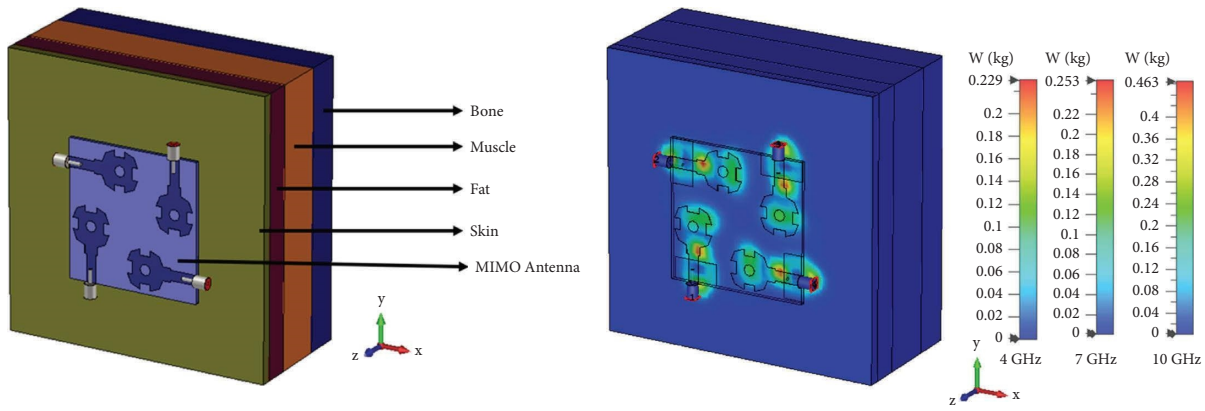

(a) (b)

Figure 19: SAR analysis of the MIMO antenna: (a) rectangular human body model and (b) SAR values.

Table 1: Tissue properties of human body.

Human body tissue layers	Frequency (GHz)	Relative permittivity (ε_r)	Loss tangent (tan δ)	Thickness of tissue layers (mm)
Skin	4	36.6	0.281	2
	7	34.1	0.36	
	10	31.3	0.47	
Fat	4	5.12	0.14	3
	7	4.85	0.19	
	10	4.6	0.24	
Muscle	4	50.8	0.23	7
	7	46.9	0.33	
	10	42.8	0.45	
Bone	4	10.5	0.16	4
	7	9.17	0.183	
	10	8.12	0.21	

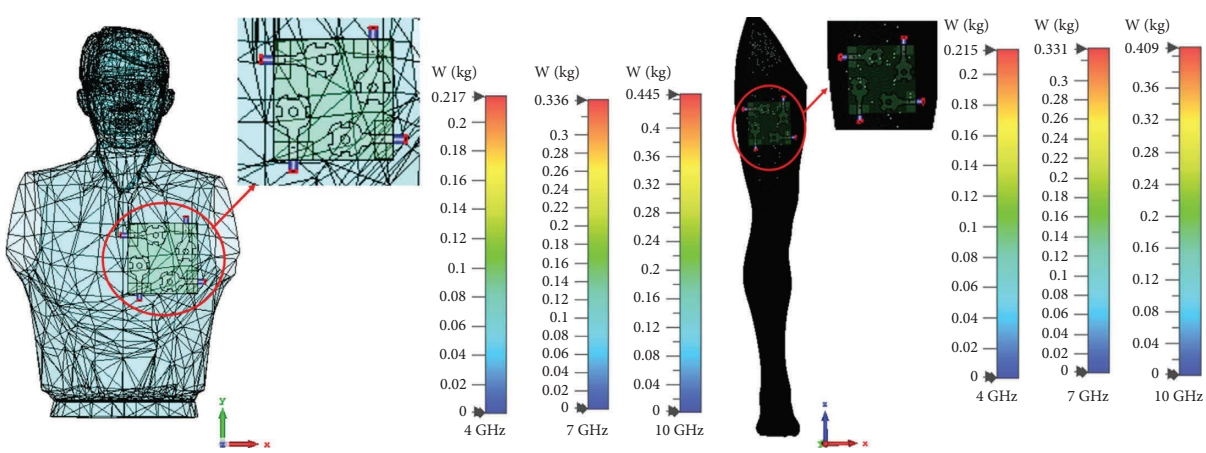

(a) (b)

Figure 20: Continued.

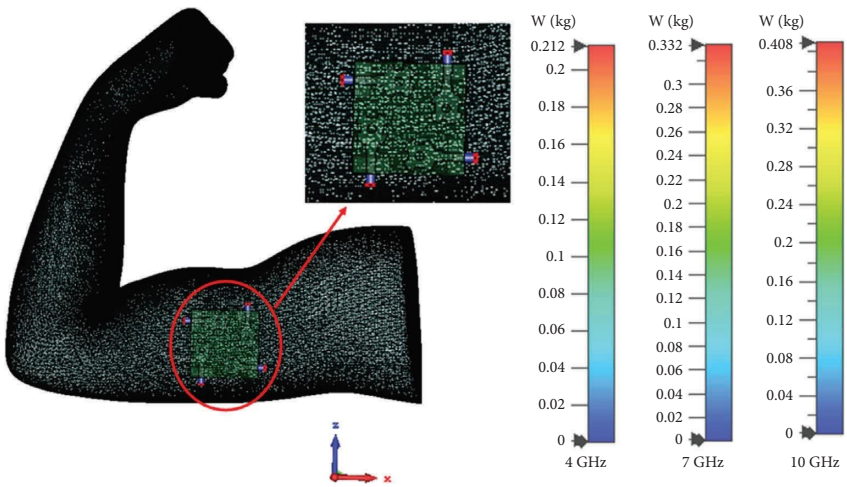

(c)

Figure 20: SAR values obtained from the open-source model: (a) chest, (b) thigh, and (c) arm.

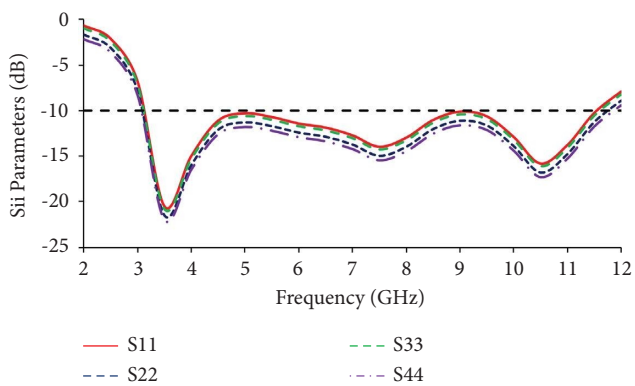

Figure 21: Simulated reflection coefficient plot for on-body analysis of the MIMO antenna.

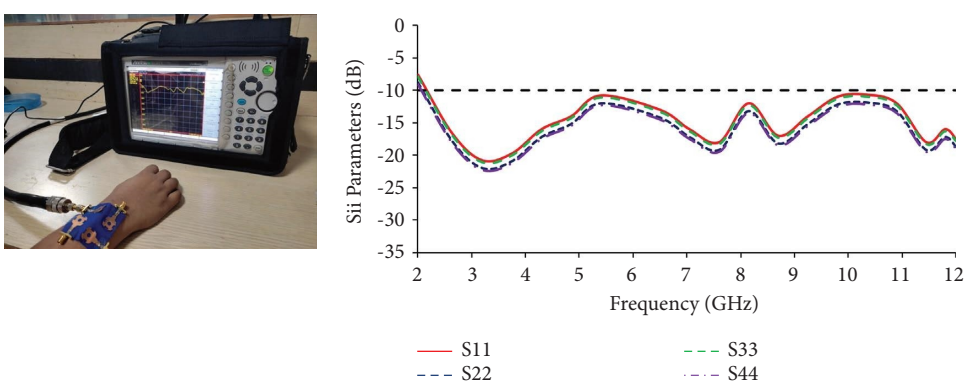

(a) (b)

Figure 22: SAR analysis of the antenna prototype (measured): (a) on-body and (b) reflection coefficients.

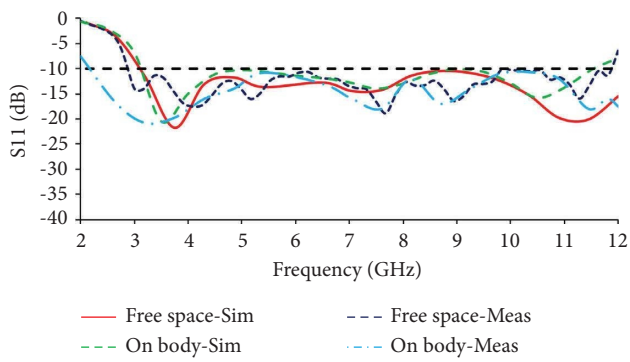

Figure 23: Reflection coefficient plots of the MIMO antenna in free space and on the body.

Table 2: Comparison of the proposed work with existing literature.

Ref.	Unit cell area (λ_0)	Frequency (GHz)	Bandwidth (GHz)	Substrate	Peak gain (dBi)	SAR analysis
[7]	0.51×0.39	2.4	0.08	Felt	4.83	Yes
[29]	0.4×0.97	0.915	0.06	Felt	2.19	—
[39]	0.06×0.24	0.915	0.03	Denim, polyester	1.88, 1.57	—
[40]	0.54×0.54	2.45, 4.25	0.23, 0.27	Leather	0.29, 3.05	—
[41]	0.32×0.57	5.8	0.15	Fabric	2.8	—
[42]	0.38×1.9	0.9	0.2	Cotton	3.25	—
[43]	0.23×0.17	2.45, 3.5, 5.5	0.19, 0.22, 2.18	FR-4	1.3, 2.9, 4.3	—
[44]	0.25×0.25	3.1–10.6	10	FR-4	4	—
[45]	0.22×0.16	3.1–10.6	11.7	FR-4	1.1-4.3	—
[46]	0.17×0.21	3.1–10.6	12	FR-4	4.3	—
[47]	0.258×0.21	3.1–10.6	8.9	Polyester	4.62	Yes
Proposed work	0.26×0.16	3.1–10.6	9.1	Cotton	4.84	Yes

(iv) In comparison to [7, 29, 39–47], the proposed antenna offers a higher gain of 4.84 dBi

4. Conclusion

In this work, a quad-port UWB MIMO antenna is presented for smart clothing applications. The antenna is made of cotton fabric that has been engineered to function as a textile antenna when combined with a patient cloth. The antenna is constructed using four similar antenna elements positioned orthogonally to improve isolation without adding decoupling structures. Over the UWB range, isolation is greater than 17 dB, and the calculated diversity characterization is comparable. Also, the proposed antenna can bend up to 20 mm, making it suitable for wearable applications. The SAR analysis of the MIMO antenna shows satisfactory values that are significantly lower than 1.6 W/Kg, making the proposed antenna suitable for patient monitoring applications.

Data Availability

The data used to support the findings are available from the corresponding author upon request.

Conflicts of Interest

The authors declare that they have no conflicts of interest.

References

[1] P. B. Samal, P. Jack Soh, and Z. Zakaria, "Compact and wearable microstrip-based textile antenna with full ground plane designed for WBAN-UWB 802.15.6 application," in *Proceedings of the 13th European Conference on Antennas and Propagation (EuCAP)*, pp. 1–4, Krakow, Poland, March, 2019.

[2] A. Iqbal, A. J. Alazemi, and N. Khaddaj Mallat, "Slot-DRA-based independent dual-band hybrid antenna for wearable biomedical devices," *IEEE Access*, vol. 7, Article ID 184029, 2019.

[3] T. N. Kapetanakis, C. D. Nikolopoulos, K. Petridis, and I. O. Vardiambasis, "Wearable textile antenna with a graphene sheet or conductive fabric patch for the 2.45 GHz band," *Electronics*, vol. 10, no. 21, p. 2571, 2021.

[4] S. Costanzo and G. Ammendola, "Compact textile wearable antenna for security applications," in *Proceedings of the 23rd International Conference on Applied Electromagnetics and Communications (ICECOM)*, pp. 1–3, Dubrovnik, Croatia, September, 2019.

[5] S. Amit, V. Talasila, and P. Shastry, "A semi-circular slot textile antenna for UltraWideband applications," in *Proceedings of the IEEE International Symposium on Antennas and Propagation and USNC-URSI Radio Science Meeting*, pp. 249-250, Atlanta, GA, USA, July, 2019.

[6] P. M. Potey and K. Tuckley, "Design of wearable textile antenna with various substrate and investigation on fabric selection," in *Proceedings of the 3rd International Conference on Microwave and Photonics (ICMAP)*, pp. 1-2, Dhanbad, India, February, 2018.

[7] R. Aprilliyani, P. A. Dzagbletey, J. H. Lee, M. J. Jang, J.-H. So, and J.-Y. Chung, "Effects of textile weaving and finishing processes on textile-based wearable patch antennas," *IEEE Access*, vol. 8, Article ID 63295, 2020.

[8] J. Zhong, A. Kiourti, T. Sebastian, Y. Bayram, and J. L. Volakis, "Conformal load-bearing spiral antenna on conductive textile threads," *IEEE Antennas and Wireless Propagation Letters*, vol. 16, pp. 230–233, 2017.

[9] A. K. Biswas, K. Roy, and U. Chakraborty, "Investigation of a four-element textile multiple input multiple output antenna for ku-band applications," in *Proceedings of the IEEE Region 10 Symposium (TENSYMP)*, pp. 382–385, Dhaka, Bangladesh, June, 2020.

[10] N. Malekpour and M. A. Honarvar, "Design of high-isolation compact MIMO antenna for UWB application," *Progress In Electromagnetics Research C*, vol. 62, pp. 119–129, 2016.

[11] H. Ben Hamadi, S. Ghnimi, L. Latrach, and A. Gharsallah, "Design of the millimeter-wave textile antenna loaded with AMC structures for 5G applications," in *Proceedings of the 32nd International Conference on Microelectronics (ICM)*, pp. 1–5, Aqaba, Jordan, December, 2020.

[12] H. Arun, A. K. Sarma, M. Kanagasabai, S. Velan, C. Raviteja, and M. G. N. Alsath, "Deployment of modified serpentine structure for mutual coupling reduction in MIMO antennas," *IEEE Antennas and Wireless Propagation Letters*, vol. 13, pp. 277–280, 2014.

[13] C. Mao, P. L. Werner, D. H. Werner, D. Vital, and S. Bhardwaj, "Dual-polarized armband embroidered textile antenna for on-/off-body wearable applications," in *Proceedings of the IEEE International Symposium on Antennas and Propagation and USNC-URSI Radio Science Meeting*, pp. 1555-1556, Atlanta, GA, USA, July, 2019.

[14] K. Do-Gu, T. Jinpil, and C. Jaehoon, "MIMO antenna with high isolation for WBAN applications," *International Journal of Antennas and Propagation*, vol. 2015, Article ID 370763, 7 pages, 2015.

[15] T. Kaufmann and C. Fumeaux, "Wearable textile half-mode substrate-integrated cavity antenna using embroidered vias," *IEEE Antennas and Wireless Propagation Letters*, vol. 12, pp. 805–808, 2013.

[16] K.-H. Wang and J.-S. Li, "Jeans textile antenna for smart wearable antenna," in *Proceedings of the 12th International Symposium on Antennas, Propagation and EM Theory (ISAPE)*, pp. 1–3, Hangzhou, China, December, 2018.

[17] S. Zhu and R. Langley, "Dual-Band wearable textile antenna on an EBG substrate," *IEEE Transactions on Antennas and Propagation*, vol. 57, no. 4, pp. 926–935, 2009.

[18] A. K. Ilyas, D. Budiastuti, and E. T. Rahardjo, "Effect of textile substrate on antenna performance for GPS application," in *Proceedings of the IEEE Region 10 Conference (TENCON)*, pp. 914–918, Osaka, Japan, November, 2020.

[19] A. Iqbal, A. Smida, A. J. Alazemi, M. I. Waly, N. Khaddaj Mallat, and S. Kim, "Wideband circularly polarized MIMO antenna for high data wearable biotelemetric devices," *IEEE Access*, vol. 8, Article ID 17935, 2020.

[20] C. G. Revati and R. R. Patil, "Slot-based mutual coupling reduction technique for MIMO antenna," *SN Computer Science*, vol. 2, pp. 104–106, 2021.

[21] I. Nadeem and D.-Y. Choi, "Study on mutual coupling reduction technique for MIMO antennas," *IEEE Access*, vol. 7, pp. 563–586, 2019.

[22] Y. S. Chen and C. P. Chang, "Design of a four-element multiple-input– multiple-output antenna for compact long-term evolution small-cell base stations," *IET Microwaves, Antennas & Propagation*, vol. 10, no. 4, pp. 385–392, 2016.

[23] L. Qian, D. Chong, Y. Ruichao et al., "Mutual coupling reduction between patch antennas using meander line," *International Journal of Antennas and Propagation*, vol. 2018, Article ID 2586382, 7 pages, 2018.

[24] A. Smida, A. Iqbal, A. J. Alazemi, M. I. Waly, R. Ghayoula, and S. Kim, "Wideband wearable antenna for biomedical telemetry applications," *IEEE Access*, vol. 8, Article ID 15687, 2020.

[25] E. Çelenk and N. T. Tokan, "All-textile on-body antenna for military applications," *IEEE Antennas and Wireless Propagation Letters*, vol. 21, no. 5, pp. 1065–1069, 2022.

[26] Y. Mukai and M. Suh, "Design and characterization of a cotton fabric antenna for on-body thermotherapy," *Journal of Industrial Textiles*, vol. 51, no. 1_suppl, pp. 1627S–1644S, 2022.

[27] K. P. Ray, "Design aspects of printed monopole antennas for ultra-wide band applications," *International Journal of Antennas and Propagation*, vol. 2008, Article ID 713858, 8 pages, 2008.

[28] R. Sanyal, P. P. Sarkar, and S. Sarkar, "Octagonal nut shaped monopole UWB antenna with sextuple band notched characteristics," *AEU-International Journal of Electronics and Communications*, vol. 110, Article ID 152833, 2019.

[29] M. E. Bakkali, M. Martinez-Estrada, R. Fernandez-Garcia, I. Gil, and O. E. Mrabet, "Effect of bending on a textile UHF-rfid tag antenna," in *Proceedings of the 14th European Conference on Antennas and Propagation (EuCAP)*, pp. 1–5, Copenhagen, Denmark, March, 2020.

[30] S. Mohandoss, S. K. Palaniswamy, R. R. Thipparaju, M. Kanagasabai, B. R. Bobbili Naga, and S. Kumar, "On the bending and time domain analysis of compact wideband flexible monopole antennas," *AEU - International Journal of Electronics and Communications*, vol. 101, pp. 168–181, 2019.

[31] G. Varshney, S. Gotra, S. Chaturvedi, V. S. Pandey, and R. S. Yaduvanshi, "Compact four-port MIMO dielectric resonator antenna with pattern diversity," *IET Microwaves, Antennas & Propagation*, vol. 13, no. 12, pp. 2193–2198, 2019.

[32] W. Mu, H. Lin, Z. Wang et al., "A flower-shaped miniaturized UWB-MIMO antenna with high isolation," *Electronics*, vol. 11, no. 14, p. 2190, 2022.

[33] S. Gotra, G. Varshney, V. S. Pandey, and R. S. Yaduvanshi, "Super-wideband multi-input–multi-output dielectric resonator antenna," *IET Microwaves, Antennas & Propagation*, vol. 14, no. 1, pp. 21–27, 2019.

[34] Y. Gao, J. Wang, X. Wang, and R. Shao, "Miniaturized MIMO antenna array with high isolation for 5G metal-frame smartphone application," *Micromachines*, vol. 13, no. 7, p. 1064, 2022.

[35] L. Kannappan, S. K. Palaniswamy, L. Wang et al., "Quad-port multiservice diversity antenna for automotive applications," *Sensors*, vol. 21, no. 24, p. 8238, 2021.

[36] M. E. Lajevardi and M. Kamyab, "Ultraminiaturized metamaterial-inspired SIW textile antenna for off-body applications," *IEEE Antennas and Wireless Propagation Letters*, vol. 16, pp. 3155–3158, 2017.

[37] S. Gabriel, R. W. Lau, and C. Gabriel, "The dielectric properties of biological tissues: II. Measurements in the frequency range 10 Hz to 20 GHz," *Physics in Medicine and Biology*, vol. 41, no. 11, pp. 2251–2269, 1996.

[38] Free3d, "3d-models human," 2022, https://free3d.com/3d-models/human.

[39] F. Lagha, S. Beldi, and L. Latrach, "Design of UHF RFID body-worn textile tag for wireless applications," in *Proceedings of*

the IEEE International Conference on Design & Test of Integrated Micro & Nano-Systems (DTS), pp. 1–4, Gammarth, Tunisia, April, 2019.

[40] J. Tak and J. Choi, "An all-textile louis vuitton logo antenna," *IEEE Antennas and Wireless Propagation Letters*, vol. 14, pp. 1211–1214, 2015.

[41] Y. Hong, J. Tak, and J. Choi, "An all-textile SIW cavity-backed circular ring-slot antenna for WBAN applications," *IEEE Antennas and Wireless Propagation Letters*, vol. 15, pp. 1995–1999, 2016.

[42] G. Ginestet, N. Brechet, J. Torres et al., "Embroidered antenna-microchip interconnections and contour antennas in passive UHF RFID textile tags," *IEEE Antennas and Wireless Propagation Letters*, vol. 16, pp. 1205–1208, 2017.

[43] B. Bayarzaya, N. Hussain, W. A. Awan et al., "A compact MIMO antenna with improved isolation for ISM, sub-6 GHz, and WLAN application," *Micromachines*, vol. 13, no. 8, p. 1355, 2022.

[44] A. Wu, M. Zhao, P. Zhang, and Z. Zhang, "A compact four-port MIMO antenna for UWB applications," *Sensors*, vol. 22, no. 15, p. 5788, 2022.

[45] A. Altaf, A. Iqbal, A. Smida et al., "Isolation improvement in UWB-MIMO antenna system using slotted stub," *Electronics*, vol. 9, no. 10, p. 1582, 2020.

[46] A. Iqbal, O. A. Saraereh, A. W. Ahmad, and S. Bashir, "Mutual coupling reduction using F-shaped stubs in UWB-MIMO antenna," *IEEE Access*, vol. 6, pp. 2755–2759, 2018.

[47] T. Govindan, S. K. Palaniswamy, M. Kanagasabai, S. Kumar, M. Marey, and H. Mostafa, "Design and analysis of a flexible smart apparel MIMO antenna for bio-healthcare applications," *Micromachines*, vol. 13, no. 11, p. 1919, 2022.